Subpixel colocalization reveals amyloid precursor protein-dependent kinesin-1 and dynein association with axonal vesicles

Lukasz Szpankowski[a,b,c], Sandra E. Encalada[b,1], and Lawrence S. B. Goldstein[b,c,2]

[a]Bioinformatics and Systems Biology Graduate Program, Department of Bioengineering, [b]Department of Cellular and Molecular Medicine, School of Medicine, and [c]Howard Hughes Medical Institute, University of California at San Diego, La Jolla, CA 92093

Edited by James A. Spudich, Stanford University School of Medicine, Stanford, CA, and approved April 4, 2012 (received for review December 12, 2011)

Intracellular transport of vesicles and organelles along microtubules is powered by kinesin and cytoplasmic dynein molecular motors. Both motors can attach to the same cargo and thus must be coordinated to ensure proper distribution of intracellular materials. Although a number of hypotheses have been proposed to explain how these motors are coordinated, considerable uncertainty remains, in part because of the absence of methods for assessing motor subunit composition on individual vesicular cargos. We developed a robust quantitative immunofluorescence method based on subpixel colocalization to elucidate relative kinesin-1 and cytoplasmic dynein motor subunit composition of individual, endogenous amyloid precursor protein (APP) vesicles in mouse hippocampal cells. The resulting method and data allow us to test a key in vivo prediction of the hypothesis that APP can recruit kinesin-1 to APP vesicles in neuronal axons. We found that APP levels are well-correlated with the amount of the light chain of kinesin-1 (KLC1) and the heavy chain of cytoplasmic dynein (DHC1) on vesicles. In addition, genetic reduction of APP diminishes KLC1 and DHC1 levels on APP cargos. Finally, our data reveal that reduction of KLC1 leads to decreased levels of DHC1 on APP vesicles, suggesting that KLC1 is necessary for the association of DHC1 to these cargos, and help to explain previously reported retrograde transport defects generated when kinesin-1 is reduced.

axonal transport | microtubule motor recruitment | Alzheimer's disease

Microtubule-based transport of vesicles and organelles in neurons is coordinated by kinesin (anterograde) and cytoplasmic dynein (retrograde) motor complexes. These motor proteins and their regulators play critical roles in long-distance signaling events in neurons, neuronal regeneration, and in the development of neurodegenerative disease (1–3). Several diseases in humans, such as hereditary spastic paraplegia (4), Charcot-Marie-Tooth type 2 (5), and ALS-like motor degeneration (6), have been linked directly to mutations in genes encoding motor proteins. Additionally, disruption of transport is thought to be an early and perhaps causative event in Alzheimer's disease, Parkinson disease, and ALS, where axonal pathologies including abnormal accumulations of proteins and organelles have been routinely observed (1).

Kinesin-1 is composed of heavy chain (KHC or KIF5) and light chain (KLC) subunits (7, 8). Motor activity is executed by KHC, and cargo binding and regulatory activities are carried out by both KHC and KLC (9–11). Dynein is a large protein complex with six subunits: a large dynein heavy chain (DHC), an intermediate and light-intermediate chain (DIC and DLIC), and three dynein light chains (DLC) (12). Several types of vesicles, including amyloid precursor protein (APP) vesicles, depend upon kinesin-1 (9, 13–17) for their anterograde movement in axons. These studies raised the possibility that APP transport and its influence on APP proteolytic processing play an important role in the development of Alzheimer's disease (1, 3, 9, 18–20).

Although much progress has been made toward elucidating underlying principles of motor coordination (21–25), we lack a full understanding of how motor subunits are recruited to APP vesicles and, moreover, how levels of these subunits on vesicles are determined. Previous work raised the possibility that APP could bind to KLC and thus kinesin-1 either directly or indirectly via complex formation with JIP1 (9, 26, 27), a proposal that has remained controversial in the field. Here, we set out to test a key in vivo prediction of the hypothesis that APP recruits kinesin-1 to vesicles by developing and implementing a rigorous method for high-throughput, subpixel colocalization of diffraction limited fluorescent puncta in 2D immunofluorescence images at a separation below the Rayleigh limit, i.e., with superresolution. Specifically, this method allowed us to assess the composition of molecular motors on endogenous axonal APP vesicles, in the absence of overexpression, because overexpression of motors, APP itself, or of vesicular proteins frequently alter vesicle behavior substantially (20, 28–30). We recently reported initial studies of motor association with mammalian prion protein (PrP^C) vesicles using an early version of this method (31), the full development and extensive validation of which we report here.

Results

Development of Fluorescence Intensity Analyses and Colocalization Methods. We developed a "Motor Colocalization" software package to measure the relative amount of motor subunits associated with any detectable vesicular cargo of interest. We applied this quantitative method to estimate the degree of colocalization between APP-containing vesicles and two motor subunits, KLC1 and DHC1, from cultured neonatal mouse primary hippocampal neurons. These cells have long, isolated axonal projections, which are particularly amenable to reproducible staining of vesicular proteins. Hippocampal cells were fixed and stained with antibodies against APP, KLC1, and DHC1. Resulting immunofluorescence images showed dense punctate vesicular staining and a high degree of colocalization between APP vesicles and motor subunits (Fig. 1*A*). Subpixel positions of fluorescent point sources were determined for each channel—APP, KLC1, DHC1—separately by iteratively fitting Gaussian kernels approximating the 2D microscope point-spread function to the diffraction limited data surrounding predetermined local maxima seeds (32, 33). Subpixel localization of particles with overlapping signal were determined by fitting multiple Gaussians simultaneously, each one representing a version of the point-spread function shifted in space, resulting in improved accuracy and resolution. The Gaussian-fitting algorithm we used is particularly suitable for situations of

Author contributions: L.S., S.E.E., and L.S.B.G. designed research; L.S. and S.E.E. performed research; L.S. and S.E.E. contributed new reagents/analytic tools; L.S., S.E.E., and L.S.B.G. analyzed data; and L.S. and L.S.B.G. wrote the paper.

The authors declare no conflict of interest.

This article is a PNAS Direct Submission.

[1]Present address: Department of Molecular and Experimental Medicine and Department of Cell Biology, Dorris Neuroscience Center, The Scripps Research Institute, La Jolla, CA, 92037.

[2]To whom correspondence should be addressed. E-mail: lgoldstein@ucsd.edu.

This article contains supporting information online at www.pnas.org/lookup/suppl/doi:10.1073/pnas.1120510109/-/DCSupplemental.

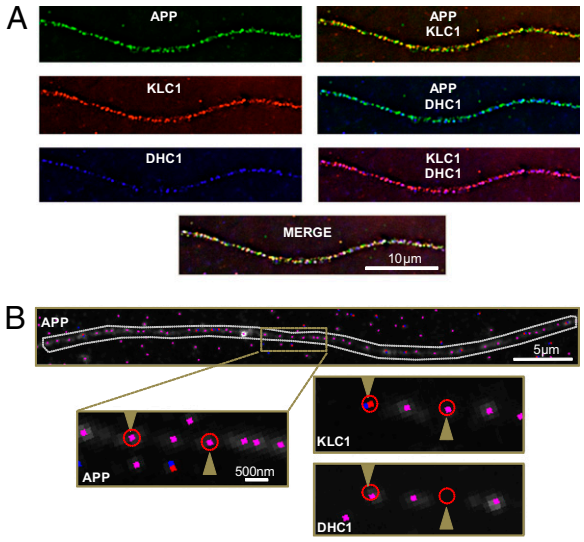

Fig. 1. Motor colocalization. (*A*) Immunofluorescence images show antibody staining of APP, KLC1, and DHC1 at 100×. (*B*, *Upper*) Detected APP features (vesicles) within an axon. Blue dots represent local maxima, red dots mark approximate (nearest pixel) position of subpixel Gaussian fits, and the overlap of blue and red is shown in pink. Gray contour denotes user-defined region of interest. (*Lower*) Enlargement of the three channels, corresponding to anti-APP (seed), anti-KLC1, and anti-DHC1 antibody staining. Red circles outline the 300-nm cutoff radius for colocalization and are centered at the precise subpixel coordinates of each APP Gaussian fitting. Arrowheads point to the position of two separate APP detected vesicles, showing association with KLC1 only (*Right*) or both KLC1 and DHC1 (*Left*).

dense particle distributions (*SI Materials and Methods*) and thus ideal for the analysis of vesicular staining in axons.

The Motor Colocalization software extracts the subpixel position information (x- and y-coordinates) from user-selected regions in any channel and reports the number of colocalization events and associated intensities from analogous optical sections within a user-defined radius (Fig. 1*B*). Robust measures of relative intensity for each detected point source within a channel were obtained directly from the amplitude of the fitted Gaussian functions, and could be accurately compared because the SD used for each Gaussian fit remains constant (see Fig. S1 for analysis of uncertainty).

For all analyses, the cutoff for subpixel colocalization was set as a 300-nm radius based on the optics, resolution limit, and relevant physical size of the vesicles and motor subunits (31). An analysis of colocalization distance suggested that the percentage of motor association with vesicles plateaus at ∼300 nm and begins to pick up motor subunit signals from adjacent APP vesicles at cutoffs greater than this selected threshold. To allow for rigorous comparison of feature intensity between experimental image data collected on different days, a normalization approach was applied using 2.5-μm diameter InSpeck beads (Invitrogen). Additionally, TetraSpeck microspheres (Invitrogen) were used to account and adjust for chromatic aberration of the different fluorescent channels (Fig. S2) so that all images could be subjected to registration correction before analysis (*SI Materials and Methods*).

Previous studies reported a linear relationship between protein amount and associated fluorescence intensity in highly controlled imaging studies (34, 35), suggesting that within a certain range, fluorescence intensity is determined by—and hence correlated to—protein amount independent of what protein is tagged by a fluorophore or where the tagged protein is localized. However, in metazoan systems, expressing tagged proteins at endogenous levels and with endogenous isoforms often results in under- or overexpression, thereby preventing accurate estimation of relative amounts of protein. Thus, an antibody-based method, although problematic for evaluation of absolute amounts of proteins in situ, is valuable for probing the relative amounts of endogenous proteins if appropriate quantitation can be established. In particular, because overexpression of tagged proteins including APP, KLC1, and DHC1 could significantly alter the transport behavior of APP (20, 29) and other vesicles in vivo, antibody staining has the advantage of avoiding the artifacts inherent in overexpression experiments.

Validation of Fluorescence Intensity Analyses and Colocalization Methods. We first validated the specificity of primary antibodies used to detect endogenous APP, KLC1, and DHC1 by reducing protein levels using either deletion mutants or through expression of shRNA constructs in WT neurons. We also determined whether the fluorescence intensity readouts of stained APP and KLC1 vesicular puncta correlated to protein levels increased by transient transfection of tagged APP and KLC1. In previous work we found that KLC1 staining intensity increased proportionally ($r = 0.99$) with *KLC1* copy number (31) for all kinesin-1–driven axonal cargo.

To investigate the motor subunit composition of APP vesicles, anti-APP staining served as the seed channel for colocalization with corresponding anti-KLC1 and anti-DHC1 signal (Fig. 1*B*). We evaluated motor-vesicle association, and therefore the specificity of KLC1 association with APP vesicles, in hippocampal neurons cultured from sibling mice with no copies of *KLC1* ($KLC1^{-/-}$), one copy ($KLC1^{+/-}$), and both copies ($KLC1^{+/+}$) in two different ways. First, as expected, when *KLC1* copy number was reduced, we observed significant decreases in the frequency of detectable KLC1 puncta found within 300 nm of a detected APP vesicle feature. For $KLC1^{+/+}$, 55.0 ± 1.4% of APP vesicles colocalized with KLC1, 42.3 ± 1.6% in $KLC1^{+/-}$, and 23.1 ± 1.2% for $KLC1^{-/-}$ genotypes (Fig. 2*A*). Although KLC1 association in null KLC1 mice did not decrease to background amounts (∼4%), presumably because of a small amount of cross-reactivity with KLC2 (*SI Materials and Methods*), a highly significant drop of ∼65% was observed. Second, to investigate changes in relative KLC1 subunit amount associated with individual APP vesicles in *KLC1* genotypes, KLC1 intensity distributions were determined for all three genotypes (Fig. 2*B*). Of note, the KLC1 intensity distribution in $KLC1^{+/+}$ animals closely followed what was observed in WT animals used as controls throughout this study. When one copy of *KLC1* was removed, we observed a significant shift to lower intensity values [<100 arbitrary units (AU)] at the expense of higher intensity features (>100 AU). Thus, when one copy of the gene is removed, most APP vesicles have less associated kinesin-1, although vesicles with multiple KLC1 subunits still exist. These multiples are less common than in the $KLC1^{+/+}$ animals, but a significant peak in smaller intensity values, presumably corresponding to fewer KLC1 subunits associated with APP vesicles, were significantly enhanced. $KLC1^{-/-}$ animals showed highly significant reductions for all KLC1 intensity values.

To further validate the specificity of the KLC1 antibody staining, cells were transfected with fluorescently labeled versions of KLC1 (KLC1-mCherry) and subsequently stained. An analysis of intensity levels showed highly significant positive correlations between transfected protein levels and associated anti-KLC1 intensities, resulting in a Pearson correlation coefficient of $r = 0.87$ (Fig. 2*C* and Fig. S3).

DHC1 antibody specificity was previously assessed by transfecting N2a cells with DHC1 shRNA, which resulted in an 80–90% decrease in message levels (31). Transfected hippocampal neurons exhibited marked decreases in DHC1 staining (Fig. S4 *A–D*). Average anti-DHC1 intensity per square micrometer in DHC1 shRNA-transfected cells was reduced by 72% compared with control nontransfected cells (Fig. S4*E*). The magnitude in observed signal reduction was analogous to decreases in protein levels assessed previously by Western blot (31), and confirmed the specificity of the selected DHC1 antibody (*SI Materials and Methods*).

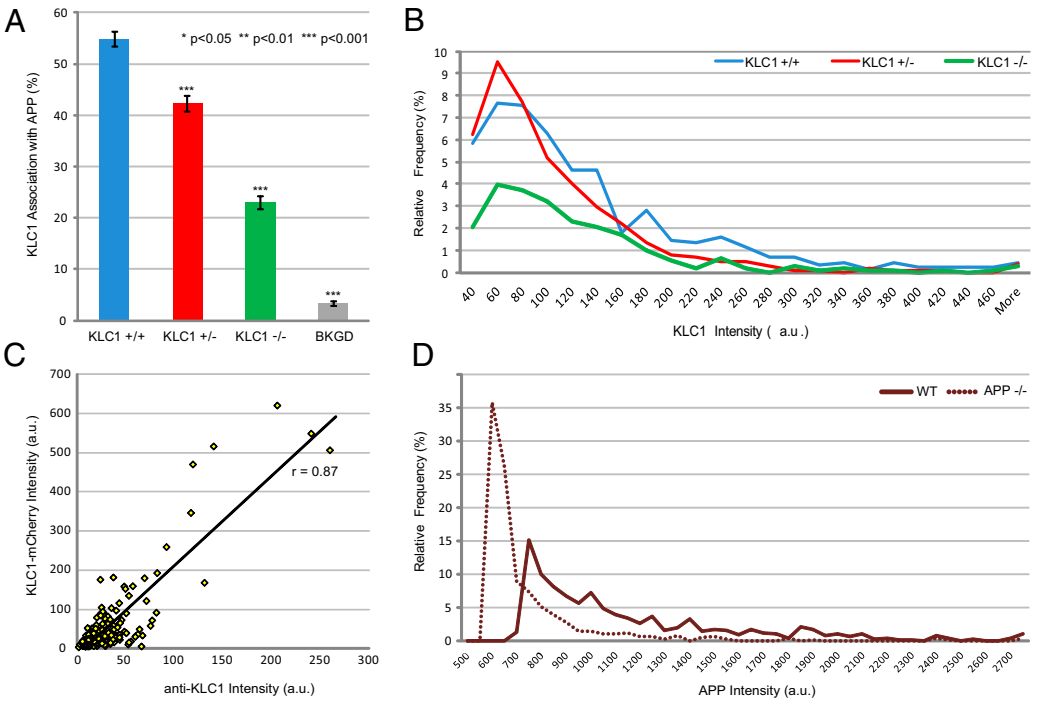

Fig. 2. (*A*) KLC1 motor subunit composition of APP vesicles in *KLC1* genotypes. $KLC1^{+/+}$: $n_{Vesicles}$ = 1,676, $n_{Animals}$ = 4, n_{Axons} = 20; $KLC1^{+/-}$: $n_{Vesicles}$ = 1,760, $n_{Animals}$ = 4, n_{Axons} = 19; $KLC1^{-/-}$: $n_{Vesicles}$ = 1,569, $n_{Animals}$ = 3, n_{Axons} = 17. BKGD denotes nonspecific colocalization of background staining between immunofluorescence channels outside of axonal projections. Error bars show SEM. (*B*) APP vesicle-associated anti-KLC1 intensity distributions in *KLC1* genotypes. Distributions are presented as a function of relative frequency of the total number of APP vesicles detected, and to simplify comparison, plotted as line graphs using an intensity bin size of 20 AU. $KLC1^{+/+}$: $n_{Vesicles}$ = 895, $n_{Animals}$ = 2, n_{Axons} = 10; $KLC1^{+/-}$: $n_{Vesicles}$ = 1,041, $n_{Animals}$ = 2, n_{Axons} = 10; $KLC1^{-/-}$: $n_{Vesicles}$ = 1,126, $n_{Animals}$ = 2, n_{Axons} = 10. Error bars show SEM. (*C*) KLC1-mCherry (seed channel) vs. associated anti-KLC1 intensity correlation in WT axons. n_{Axons} = 3, $n_{KLC1\text{-}mCherry}$ = 271. (*D*) Anti-APP intensity distributions in *APP* genotypes. WT: n_{Axons} = 4; $APP^{-/-}$: n_{Axons} = 3. The upward intensity shift in anti-APP dynamic range is a result of increased exposure settings required to detect the low-level background APP signal in $APP^{-/-}$ cells. Bin size = 50 AU.

To validate the specificity of the APP antibody, cells were transfected with fluorescently labeled versions of APP (APP-YFP) and subsequently stained with anti-APP. Analysis of intensity levels revealed highly significant positive correlations between transfected protein levels and APP immunofluorescence intensities with a Pearson correlation coefficient of r = 0.74. In animals lacking both copies of *APP* ($APP^{-/-}$), a 72.1% drop in APP antibody signal intensity was observed (Fig. 2*D*), approximating background fluorescence levels. Additionally, we directly compared Gaussian fitting in conventional microscopy images to superresolution imaging and observed highly comparable results (*SI Text*). These observations validate the specificity of the selected antibody probes and suggest that relative estimates of protein amount can be reliably extracted from our immunofluorescence measurements.

Levels of Kinesin-1 and Dynein Associated with APP Vesicles Are Proportional to APP Levels. Although APP vesicles are bidirectionally transported in mouse hippocampal axons and KLC1 is one of the anterograde motor subunits involved in this movement (20), the motors required for retrograde transport of APP vesicles have not been established. A crucial prediction of the hypothesis that APP acts as a bridge to recruit kinesin-1 to vesicles is that the amount of kinesin-1 on axonal vesicles should depend upon, and be proportional to the amount of APP in the vesicles. To test this hypothesis and to ascertain whether DHC1 subunits associate with APP vesicles, we characterized kinesin-1 (KLC1) and dynein (DHC1) association with APP vesicles in WT axons. We found that 70.5 ± 1.2% of APP vesicles colocalized with KLC1, 49.5 ± 1.1% associated with DHC1, and 38.5 ± 1.1% of APP vesicles were associated with both motor subunits (Fig. 3*A*). We did not detect any motor subunits on 18.5 ± 1.0% of APP cargos. These data support DHC1 as a putative retrograde APP vesicle motor subunit (17) and further suggest that both anterograde and retrograde motors can simultaneously associate with these vesicles.

The intensity profile of APP vesicles in WT axons resulted in a nonnormal, right-skewed distribution. To analyze this distribution further, we used a comprehensive clustering strategy to reveal normally distributed component-intensity profiles determined using the MCLUST function followed by Bayesian Information Criterion selection (36). The model-based clustering analysis predicted that vesicular APP levels are best described as a series of four normally distributed clusters (Fig. 3*B*). The means of each mode roughly correlated to 1×, 2×, 4×, and 6× levels of APP vesicle intensity, which can be interpreted as multiples of the amount of APP associated with axonal vesicles. Each individual intensity measure was classified into its respective mode by calculating classification thresholds (*SI Materials and Methods*). Hence, cluster 1 represents APP vesicles corresponding to the lowest intensity group, and higher clusters contain vesicles with increasing intensity readouts corresponding to higher APP concentrations.

Notably, the percent of KLC1 and DHC1 associated with APP increased proportionally with APP amount as evaluated by each intensity cluster (Fig. 3*C*). In cluster 1, 61.6 ± 2.1% of APP vesicles were found to be associated with the KLC1 subunit of kinesin-1, 65.7 ± 1.6% in cluster 2, 74.3 ± 1.8% in cluster 3, and 77.8 ± 2.6% in cluster 4. This result suggests that APP plays a role in recruiting KLC1 subunits to the vesicle. Our data additionally indicated that DHC1 subunit association with APP scales with increasing intensity cluster, similar to the effect noted for the light chain of kinesin-1. APP vesicles belonging to cluster 1 resulted in a 42.2 ± 1.4% colocalization with DHC1, 47.3 ± 2.0% for cluster 2, 52.0 ± 1.8% in cluster 3, and 62.8 ± 2.5% of

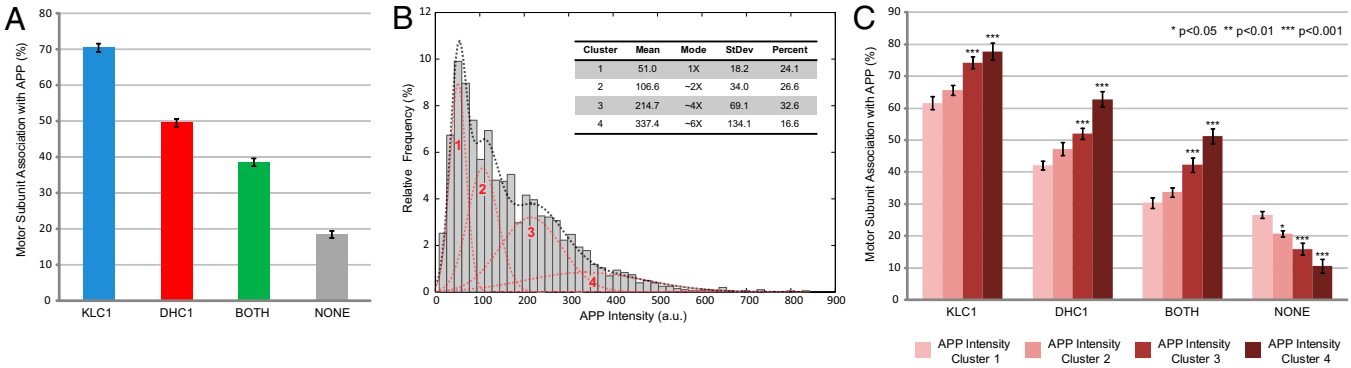

Fig. 3. (*A*) Motor subunit composition of APP vesicles in WT axons. $n_{Vesicles}$ = 4,050, $n_{Animals}$ = 6, n_{Axons} = 34. (*B*) The APP intensity profile in WT axons is described by a series of four normally distributed clusters (red curves). $n_{Vesicles}$ = 2,020, $n_{Animals}$ = 3, n_{Axons} = 17. Bin number = 50. (*C*) Motor subunit association with APP vesicles as a function of APP intensity. Error bars show SEM.

DHC1 subunits associated with cluster 4 vesicles, suggesting that APP might also recruit dynein to vesicles.

To further evaluate whether increasing levels of APP correlate with increasing amounts of motor proteins associated with these vesicles, we plotted the correlation of associated intensities for three of the designated categories of cargos; APP vesicles that had KLC1 only, DHC1 only, or both motor subunits (Fig. S5). We found a statistically significant correlation between APP-KLC1 (r = 0.56), APP-DHC1 (r = 0.24), and KLC1-DHC1 (r = 0.34) intensity values.

The distribution of APP-associated KLC1 and DHC1 intensities were nonnormal and skewed to the right (Fig. S6). Intriguingly, clustering the KLC1 intensity distribution resulted in predicted modal peaks that approximately followed a 1:2:3:6 ratio, presumably corresponding to multiples of KLC1 associated with detected APP vesicles. It is possible that we do not see 4×, 5× quantiles because at higher intensities we do not have enough datapoints to distinguish these modes and assign statistically significant clusters to them. Similarly, clustering the APP-associated DHC1 intensity distribution resulted in four separate modes that followed a 1:2:4:9 ratio, suggesting that multiple amounts of DHC1 are associated with APP vesicles in axons as well.

Genetic Reduction of APP Levels Results in Reduced Motor-Vesicle Association. To further test the hypothesis that APP is involved in recruiting KLC1 and DHC1 to vesicles, we characterized the motor subunit composition of APP vesicles in mutant mice with a single copy of *APP* ($APP^{+/-}$). We predicted that decreased APP levels would result in reduced motor subunit recruitment. Indeed, we observe that only 40.1 ± 1.4% of APP vesicles in $APP^{+/-}$ axons are associated with KLC1, a 43.1% reduction in motor subunit presence compared with WT neurons (Fig. 4*A*). DHC1 association to APP vesicles was reduced by 27.7% from WT to 35.8 ± 1.5% and accordingly only 15.1 ± 0.8% of vesicles are found to have both subunits. Of note, our data revealed no significant difference in the number of APP vesicles per micrometer of axon when one copy of *APP* is removed (WT: 1.03 APP/μm; $APP^{+/-}$: 0.98 APP/μm).

Strikingly, we observed an increase in the overall intensity profile of APP in $APP^{+/-}$ axons, because of the appearance of substantial numbers of exceptionally large and bright APP puncta (Figs. S7 and 4*B*). We interpreted these swellings as potential traffic jams or APP accumulations, possibly as a result of axonal transport deficits in these mutant neurons. This phenotype is consistent and reproducible and indicated that 11.7% of APP features detected in $APP^{+/-}$ axons fall into this category compared with only 1.1% observed in control conditions. To categorize APP puncta as swellings, a cutoff was determined by establishing that APP accumulations displayed Gaussian-intensity amplitudes greater than a μ+3σ value obtained from the analogous WT APP intensity profile. As expected, lower APP intensities are slightly enriched in the heterozygotes. We suspect that there is a small population of APP vesicles with intensities that fall below the threshold of detection in both WT and $APP^{+/-}$ genotypes. This bias presumably affects the latter condition more severely and helps explain the milder shift to lower intensities than expected.

KLC1 has been shown to be involved in the transport of a variety of cargos in axons (8, 31, 37). To probe the effect of APP reduction, the percentage of KLC1 cargos that contain APP was determined (Fig. 4*C*). In control, 64.7 ± 3.8% of KLC1 in the axon was associated with APP vesicles, and $APP^{+/-}$ axons showed significant reductions to 43.5 ± 3.9%. This observation indicates that when APP levels are reduced, a significantly

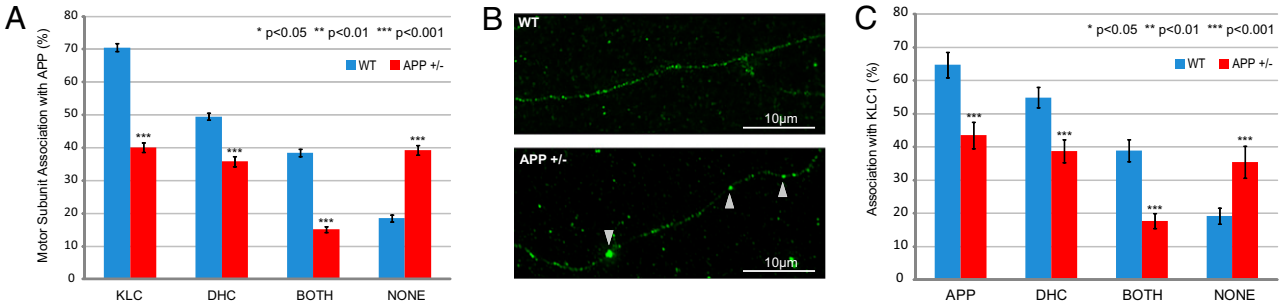

Fig. 4. (*A*) Motor subunit composition of APP vesicles in *APP* genotypes. (*B*) Representative immunofluorescence images from WT and $APP^{+/-}$ axons showing anti-APP vesicular staining. Swellings in $APP^{+/-}$ axons are indicated by the arrows. (*C*) Percentage of KLC1 cargo associated with APP or DHC1. WT: n_{Axons} = 5, n_{KLC1} = 550; $APP^{+/-}$: n_{Axons} = 5, n_{KLC1} = 324. Error bars show SEM.

smaller percentage of total KLC1-driven cargos contain APP. The corresponding increase in KLC1-associated non-APP cargos suggests competition for kinesin-1 recruitment.

Relative Dynein Motor Composition on APP Vesicles Depends upon the Amount of KLC1. To further understand APP vesicle-motor subunit association, we investigated the role that KLC1 plays in determining the amount of DHC1 on APP vesicles. Previous work found impairment of retrograde transport following reduction or inhibition of kinesin-1, suggesting coordination between opposite-polarity motors (17, 31, 38–41). We tested whether retrograde transport defects caused by reduced kinesin-1 function might be a result of decreased dynein association with APP vesicles. We found significant reductions of DHC1 subunit association as a function of decreasing *KLC1* copy number. In $KLC1^{+/+}$, 48.9 ± 1.5% of APP-containing vesicles are associated with DHC1, 37.2 ± 2.1% in $KLC1^{+/-}$, and 33.0 ± 1.0% in $KLC1^{-/-}$ animals (Fig. 5*A*). Thus, our data show that the percentage of DHC1 associated with APP vesicles significantly decrease as KLC1 levels are reduced. To investigate relative levels of DHC1 as a function of *KLC1* gene dose, we evaluated the APP-associated DHC1 intensity amplitude distributions (Fig. 5*B*) and noticed a significant decrease in the percentage of APP vesicles associated with multiple DHC1 subunits (intensity > 180 AU) when one copy of *KLC1* is removed.

Discussion

Understanding the mechanisms and regulation of vesicle and organelle movement requires detailed knowledge of motor protein composition on individual cargos. Thus, we implemented a robust subpixel detection method, developed a set of algorithms for colocalization into an easy-to-use software package, and applied the package to an analysis of motor subunit composition of APP axonal vesicles. Several validation experiments established that our colocalization and intensity analyses were reliable. The resulting data indicated that kinesin-1 and dynein levels on APP vesicles depend upon the amount of APP in those vesicles. Thus, a key in vivo prediction of the hypothesis that one of the functions of APP is to recruit motor proteins to vesicles is supported.

In comparison with previous methods, our approach has the benefit that if high-quality antibodies for vesicular proteins are available, or if genetic methods can be used to achieve normal levels of tagged protein expression, then reliable information about endogenous proteins on individual vesicles in the absence of substantial overexpression can be obtained. Hence, distribution analyses, genetic manipulations of endogenous factors, and analyses of vesicles previously observed in living cells can be achieved (31). Our method can be applied to a variety of systems that require evaluation of association between any number of tagged proteins or cellular features from diffraction-limited imaging data.

Although biochemical approaches have been used to isolate vesicular cargos followed by quantitative analysis of motor protein levels by Western blot (21, 42, 43), these data are often highly variable, resulting in data that are difficult to interpret. Additionally, this type of "bulk" analysis does not shed light on relative motor composition on the individual cargo level, but rather of an entire population, limiting the amount of information that can be extracted because motor number may vary from cargo to cargo or on single cargos over time. Other studies have attempted to infer motor number from cargo velocity in vivo, with faster cargos assumed to have more motors engaged (23, 44, 45). However, the interpretation of this indirect measure is likely complex because the loads that cargos experience in vivo may not be high enough to explain observed velocity variations, and it is unresolved whether velocities are also modulated by regulatory factors. Attempts to determine motor number on individual cargo more directly by using stall-force measurements have also been conducted (24); however, these experiments are technically challenging and not suitable for most cargos, in particular vesicles from intact axons. Moreover, direct-force measurements used to determine the number of actively engaged motors on a particular cargo provide little insight into overall motor composition of these cargos and, hence, little information about mechanisms regulating motor activation or motor recruitment to cargos. Because vesicles switch directions and presumably alter which motor or set of motors are actively engaged in millisecond time frames, achieving estimates of overall motor composition is critical to elucidating underlying association and coordination mechanisms at the individual cargo level.

APP-Dependent Recruitment of KLC1 and DHC1 to Vesicles. Reports of a direct interaction between APP and KLC1 (9), combined with genetic and other evidence (20, 28, 29, 46), led to the hypothesis that APP can serve as a vesicle adaptor for kinesin-1 via its interaction with KLC1, and thus play a role in the recruitment of kinesin-1 to axonal vesicles. More recent evidence suggests that the attachment of APP to kinesin-1 may not be direct, but instead may require proteins of the c-Jun N-terminal kinase (JNK)-interacting proteins, specifically JIP-1/JIP-2 (26, 27). In either case, the amount of APP is suggested to play a role in determining the amount of kinesin-1 on a vesicle and, therefore, the details of the movement behavior of that vesicle. Our localization and intensity analyses support the view that APP plays a role in recruiting kinesin-1 and is thus consistent with the vast majority of published evidence. Whether this recruitment is achieved through direct or indirect association was not addressed.

Our results indicate that APP also recruits DHC1 and that levels of this dynein subunit depend on KLC1 amount on the vesicle, thus suggesting a mechanism that can explain earlier

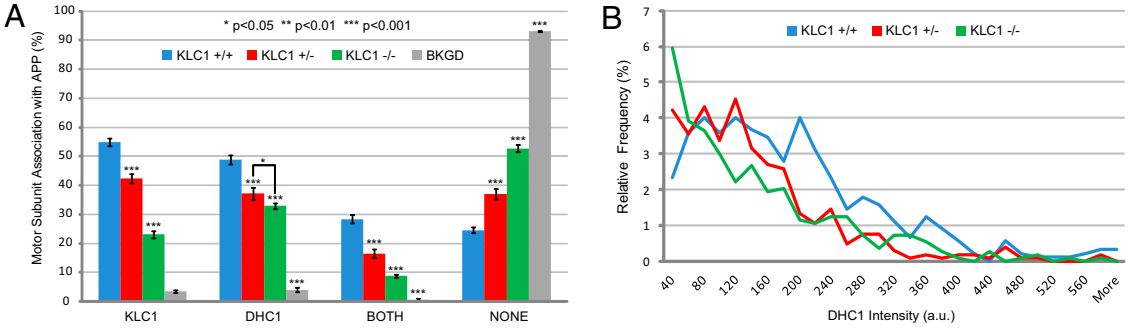

Fig. 5. (*A*) Motor subunit composition of APP vesicles in *KLC1* genotypes. $KLC1^{+/+}$: $n_{Vesicles}$ = 1,676, $n_{Animals}$ = 4, n_{Axons} = 20; $KLC1^{+/-}$: $n_{Vesicles}$ = 1,760, $n_{Animals}$ = 4, n_{Axons} = 19; $KLC1^{-/-}$: $n_{Vesicles}$ = 1,569, $n_{Animals}$ = 3, n_{Axons} = 17. Error bars show SEM. (*B*) APP vesicle-associated anti-DHC1 intensity distributions in *KLC1* genotypes. $KLC1^{+/+}$: $n_{Vesicles}$ = 895, $n_{Animals}$ = 2, n_{Axons} = 10; $KLC1^{+/-}$: $n_{Vesicles}$ = 1,041, $n_{Animals}$ = 2, n_{Axons} = 10; $KLC1^{-/-}$: $n_{Vesicles}$ = 1,126, $n_{Animals}$ = 2, n_{Axons} = 10. Bin size = 20 AU.

reports showing that reducing kinesin-1 function results in retrograde impairment (31, 38–41). These findings provide evidence for coordination between the opposite polarity motors kinesin-1 and cytoplasmic dynein, in which kinesin-1—via KLC1—is involved in the association of DHC1 to APP vesicles. Our data therefore support an association-impairment hypothesis (Fig. S8 and *SI Text*), which posits that kinesin-1 is required for proper association of dynein on APP vesicles and that loss of kinesin-1 on cargos leads to reduced dynein on vesicles.

Materials and Methods

Mice and Cell Culture. Hippocampal cultures from C57BL/6 mice were plated from either embryonic day 15–18 or 1-d-old pups (*SI Materials and Methods*). All animal protocols were approved by the Institutional Animal Care and Use Committee of the University of California at San Diego.

Immunofluorescence and Microscopy. Neurons were fixed with paraformaldehyde, permeabilized, and stained as previously described (31). All images used for analysis were obtained at 100× using a DeltaVision RT Deconvolution imaging system; however, only raw, nondeconvolved data were subject to analysis (*SI Materials and Methods*).

Motor Colocalization. After subpixel detection of fluorescent point sources, colocalization of puncta between analogous channels was determined using a 300-nm cutoff radius. All software was implemented in MATLAB (MathWorks) (*SI Materials and Methods*).

Statistics. Normality for each parameter was assessed and statistical significance ($P < 0.05$) was subsequently determined using appropriate parametric or nonparametric tests. Intensity amplitudes were clustered using the MCLUST package in R (36) (*SI Materials and Methods*).

ACKNOWLEDGMENTS. We thank Khuloud Jaqaman, Gaudenz Danuser, and Daniel Whisler for assistance with development and implementation of software; Liz Roberts for technical assistance; Brian Guzik for the light chain of kinesin-1–mCherry construct; and Jennifer Meerloo for assistance with imaging (University of California at San Diego Neuroscience Microscopy Shared Facility Grant P30 NS047101). This work was supported in part by National Institutes of Health-National Institute on Aging Grant AG032180 (to L.S.B.G.); a Damon Runyon Cancer Research Foundation Postdoctoral Fellowship (to S.E.E.); National Institutes of Health Neuroplasticity Training Grant AG000216 (to S.E.E.); and National Institutes of Health Bioinformatics Training Grant T32 GM008806 (to L.S.). L.S.B.G. is a Howard Hughes Medical Institute investigator.

1. Goldstein LS (2003) Do disorders of movement cause movement disorders and dementia? *Neuron* 40:415–425.
2. Hirokawa N, Noda Y, Tanaka Y, Niwa S (2009) Kinesin superfamily motor proteins and intracellular transport. *Nat Rev Mol Cell Biol* 10:682–696.
3. De Vos KJ, Grierson AJ, Ackerley S, Miller CC (2008) Role of axonal transport in neurodegenerative diseases. *Annu Rev Neurosci* 31:151–173.
4. Reid E, et al. (2002) A kinesin heavy chain (KIF5A) mutation in hereditary spastic paraplegia (SPG10). *Am J Hum Genet* 71:1189–1194.
5. Zhao C, et al. (2001) Charcot-Marie-Tooth disease type 2A caused by mutation in a microtubule motor KIF1Bbeta. *Cell* 105:587–597.
6. Puls I, et al. (2003) Mutant dynactin in motor neuron disease. *Nat Genet* 33:455–456.
7. Goldstein LS, Yang Z (2000) Microtubule-based transport systems in neurons: The roles of kinesins and dyneins. *Annu Rev Neurosci* 23:39–71.
8. Hirokawa N, Takemura R (2005) Molecular motors and mechanisms of directional transport in neurons. *Nat Rev Neurosci* 6:201–214.
9. Kamal A, Stokin GB, Yang Z, Xia CH, Goldstein LS (2000) Axonal transport of amyloid precursor protein is mediated by direct binding to the kinesin light chain subunit of kinesin-I. *Neuron* 28:449–459.
10. Adio S, Reth J, Bathe F, Woehlke G (2006) Review: Regulation mechanisms of Kinesin-1. *J Muscle Res Cell Motil* 27:153–160.
11. Goldstein LS, Philp AV (1999) The road less traveled: Emerging principles of kinesin motor utilization. *Annu Rev Cell Dev Biol* 15:141–183.
12. Vallee RB, Williams JC, Varma D, Barnhart LE (2004) Dynein: An ancient motor protein involved in multiple modes of transport. *J Neurobiol* 58:189–200.
13. Koo EH, et al. (1990) Precursor of amyloid protein in Alzheimer disease undergoes fast anterograde axonal transport. *Proc Natl Acad Sci USA* 87:1561–1565.
14. Amaratunga A, Morin PJ, Kosik KS, Fine RE (1993) Inhibition of kinesin synthesis and rapid anterograde axonal transport in vivo by an antisense oligonucleotide. *J Biol Chem* 268:17427–17430.
15. Szodorai A, et al. (2009) APP anterograde transport requires Rab3A GTPase activity for assembly of the transport vesicle. *J Neurosci* 29:14534–14544.
16. Kaether C, Skehel P, Dotti CG (2000) Axonal membrane proteins are transported in distinct carriers: A two-color video microscopy study in cultured hippocampal neurons. *Mol Biol Cell* 11:1213–1224.
17. Reis GF, et al. (2012) Molecular motor function in axonal transport in vivo probed by genetic and computational analysis in *Drosophila*. *Mol Biol Cell*, 10.1091/mbc.E11-11-0938.
18. Kamal A, Almenar-Queralt A, LeBlanc JF, Roberts EA, Goldstein LS (2001) Kinesin-mediated axonal transport of a membrane compartment containing beta-secretase and presenilin-1 requires APP. *Nature* 414:643–648.
19. Brunholz S, et al. (2012) Axonal transport of APP and the spatial regulation of APP cleavage and function in neuronal cells. *Exp Brain Res* 217:353–364.
20. Stokin GB, et al. (2005) Axonopathy and transport deficits early in the pathogenesis of Alzheimer's disease. *Science* 307:1282–1288.
21. Gross SP, et al. (2002) Interactions and regulation of molecular motors in *Xenopus melanophores*. *J Cell Biol* 156:855–865.
22. Welte MA (2004) Bidirectional transport along microtubules. *Curr Biol* 14:R525–R537.
23. Kural C, et al. (2005) Kinesin and dynein move a peroxisome in vivo: A tug-of-war or coordinated movement? *Science* 308:1469–1472.
24. Shubeita GT, et al. (2008) Consequences of motor copy number on the intracellular transport of kinesin-1-driven lipid droplets. *Cell* 135:1098–1107.
25. Soppina V, Rai AK, Ramaiya AJ, Barak P, Mallik R (2009) Tug-of-war between dissimilar teams of microtubule motors regulates transport and fission of endosomes. *Proc Natl Acad Sci USA* 106:19381–19386.
26. Inomata H, et al. (2003) A scaffold protein JIP-1b enhances amyloid precursor protein phosphorylation by JNK and its association with kinesin light chain 1. *J Biol Chem* 278:22946–22955.
27. Matsuda S, Matsuda Y, D'Adamio L (2003) Amyloid beta protein precursor (AbetaPP), but not AbetaPP-like protein 2, is bridged to the kinesin light chain by the scaffold protein JNK-interacting protein 1. *J Biol Chem* 278:38601–38606.
28. Torroja L, Chu H, Kotovsky I, White K (1999) Neuronal overexpression of APPL, the Drosophila homologue of the amyloid precursor protein (APP), disrupts axonal transport. *Curr Biol* 9:489–492.
29. Gunawardena S, Goldstein LS (2001) Disruption of axonal transport and neuronal viability by amyloid precursor protein mutations in *Drosophila*. *Neuron* 32:389–401.
30. King SJ, Brown CL, Maier KC, Quintyne NJ, Schroer TA (2003) Analysis of the dynein-dynactin interaction in vitro and in vivo. *Mol Biol Cell* 14:5089–5097.
31. Encalada SE, Szpankowski L, Xia CH, Goldstein LS (2011) Stable kinesin and dynein assemblies drive the axonal transport of mammalian prion protein vesicles. *Cell* 144:551–565.
32. Thomann D, Rines DR, Sorger PK, Danuser G (2002) Automatic fluorescent tag detection in 3D with super-resolution: Application to the analysis of chromosome movement. *J Microsc* 208:49–64.
33. Jaqaman K, et al. (2008) Robust single-particle tracking in live-cell time-lapse sequences. *Nat Methods* 5:695–702.
34. Geng J, Baba M, Nair U, Klionsky DJ (2008) Quantitative analysis of autophagy-related protein stoichiometry by fluorescence microscopy. *J Cell Biol* 182:129–140.
35. Wu JQ, Pollard TD (2005) Counting cytokinesis proteins globally and locally in fission yeast. *Science* 310:310–314.
36. Fraley C, Raftery AE (1999) MCLUST: Software for model based cluster analysis. *J. Classification* 16:297–306.
37. Verhey KJ, et al. (2001) Cargo of kinesin identified as JIP scaffolding proteins and associated signaling molecules. *J Cell Biol* 152:959–970.
38. Brady ST, Pfister KK, Bloom GS (1990) A monoclonal antibody against kinesin inhibits both anterograde and retrograde fast axonal transport in squid axoplasm. *Proc Natl Acad Sci USA* 87:1061–1065.
39. Pilling AD, Horiuchi D, Lively CM, Saxton WM (2006) Kinesin-1 and Dynein are the primary motors for fast transport of mitochondria in *Drosophila* motor axons. *Mol Biol Cell* 17:2057–2068.
40. Colin E, et al. (2008) Huntingtin phosphorylation acts as a molecular switch for anterograde/retrograde transport in neurons. *EMBO J* 27:2124–2134.
41. Martin M, et al. (1999) Cytoplasmic dynein, the dynactin complex, and kinesin are interdependent and essential for fast axonal transport. *Mol Biol Cell* 10:3717–3728.
42. Radtke K, et al. (2010) Plus- and minus-end directed microtubule motors bind simultaneously to herpes simplex virus capsids using different inner tegument structures. *PLoS Pathog* 6:e1000991.
43. Hendricks AG, et al. (2010) Motor coordination via a tug-of-war mechanism drives bidirectional vesicle transport. *Curr Biol* 20:697–702.
44. Hill DB, Plaza MJ, Bonin K, Holzwarth G (2004) Fast vesicle transport in PC12 neurites: Velocities and forces. *Eur Biophys J* 33:623–632.
45. Levi V, Serpinskaya AS, Gratton E, Gelfand V (2006) Organelle transport along microtubules in *Xenopus melanophores*: Evidence for cooperation between multiple motors. *Biophys J* 90:318–327.
46. Satpute-Krishnan P, DeGiorgis JA, Conley MP, Jang M, Bearer EL (2006) A peptide zipcode sufficient for anterograde transport within amyloid precursor protein. *Proc Natl Acad Sci USA* 103:16532–16537.